



OPEN Biomechanical evaluation of the new intramedullary system II for treating reverse obliquity trochanteric fractures

Qian Wang, Lu Liu, Zhong Li, Kun Zhang & Qiang Huang

Intramedullary nails are recommended for treating reverse obliquity trochanteric fractures (ROTf) in recent years. Yet, the rate of fixation failure caused by traditional intramedullary nails for managing such fractures is high. To solve this issue, the New Intramedullary System-II (NIS-II) was created. Three variations of ROTf model (AO/OTA 31-A3) were built using finite element method. Four lengthened implants were depicted and assembled on the ROTf models, comprising the Proximal Femoral Nail Antirotation (PFNA), the InterTAN nail (ITN), the Proximal Femoral Bionic Nail (PFBN), and the NIS-II. The mesh size of finite element was determined by a convergence test. The models were validated via testing axial stiffness and comparing it with published data of biomechanical experiments. Two kinds of von Mises stress and displacement were evaluated under axial loads of 2,100 N. Among the four fixation models, the NIS-II model exhibited the best biomechanical stability. Specifically, in comparison with the PFNA models, the NIS-II models demonstrated a 9.0–11.2% reduction for maximal displacement and a 9.9–12.4% reduction for maximal displacement of fracture surface (MDFS). Besides, the NIS-II models indicated a 50.1–63.7% reduction for maximal stress on implants and a 32.6–38.9% reduction for maximal stress on femurs, compared with the PFNA models. The indicators, including maximal displacement, MDFS, and maximal stress on femurs, showed statistical difference between the PFNA and NIS-II groups ($p < 0.05$). The New Intramedullary System-II showed the most superior stress distribution and the overall mechanical stability, followed by PFBN, ITN, and PFNA in fixing ROTfs under axial loads. Accordingly, the design of NIS-II is feasible and this implant could be a new choice for the treatment of ROTfs.

Keywords Reverse obliquity, Finite element, Load, Stress, Intramedullary, Trochanteric fracture, Biomechanical

The main fracture line of the reverse obliquity trochanteric fractures (ROTfs) is in the direction of proximal-medial to distal-lateral¹. This type of fracture is marked as 31-A3 in the AO/OTA classification system², and accounts for 5.3–23.5% of all trochanteric fractures^{1–5}. Elderly patients of ROTfs are usually caused by falls, while young patients result from high-energy injuries. The fracture fragments of ROTfs are prone to displacement, therefore they are classified as unstable fractures. For most ROTf patients, surgical treatment can significantly improve prognosis and the surgery is recommended to be performed within 48 h. However, there is still controversy among scholars regarding which type of implants should be used to treat such fractures.

Extramedullary implants, such as sliding hip screws, have been almost abandoned due to the high incidence of complications in treating ROTfs. Lots of scholars have recommended intramedullary nails due to their good mechanical properties and relatively low failure incidences^{6–8}. Compared to extramedullary implants, intramedullary nails have shorter level arm. Besides, for most of the time minimally invasive insertion of intramedullary implants is possible. The commonly used intramedullary nails in clinical work for managing ROTfs include PFNA, Gamma nail and ITN. Yet, complications, such as mid-shaft migration or screw cutout, are not uncommon in ROTf patients when using PFNA or similar devices^{5,9}. PFBN is a novel internal implant used for fixing femoral trochanteric fractures¹⁰. Finite element studies have shown that the biomechanical stability of PFBN (maximal stress on implants: 506.33 MPa; maximal displacement: 17.59 mm) is superior to that of PFNA (676.44 MPa; 17.63 mm), Gamma nail (956.15 MPa; 18.14 mm), and ITN (695.14 MPa; 18.23 mm).

Department of Orthopedics, Honghui Hospital, Xi'an Jiaotong University, Xi'an 710054, Shaanxi, China. ✉email: 369292735@qq.com

in fixing ROTFs under the same boundary conditions¹¹. Yet, although PFBN is designed as a triangular support structure, its effects on restricting the displacement of the fracture site of ROTFs is limited. To resist the sliding of fracture fragments, several surgeons use one or two cerclage cables to tie the fracture site of ROTFs^{12,13}. The auxiliary cable technique does enhance the fixation stability, but it increases surgical trauma and bleeding, and also increases the incidence of postoperative infections^{14,15}. Currently, there is a lack of internal implants that could provide good mechanical stability for ROTFs.

On the basis of these factors, our team created the New Intramedullary System-II (NIS-II, Fig. 1) specially for the treatment of ROTFs. In previous studies, we have designed the NIS and validated its effectiveness in the treatment of trochanteric fractures via an AO/OTA 31-A2.3 fracture model¹⁶. In this study, we optimized the direction of the subtrochanteric screw in NIS and named it NIS-II. The proximal part of the NIS-II consists of three screws and a sleeve. Two neck screws pass through the sleeve and are fixed in the femoral head at an acute angle of 7.5 degrees. The sleeve, the main nail, and the subtrochanteric screw form a triangular stable structure. Compared to the PFNA and ITN, this design might provide better axial support. Although the proximal design of PFBN also has a triangular structure, it is located above the main fracture line of ROTFs. Unlike this, the triangular structure of NIS-II is located on the fracture line. It can be approximated as “locking” the main fracture line within the triangular structure of NIS-II. This design may be able to better limit the displacement of the fracture site of ROTFs. The subtrochanteric screw passes through the sleeve and is fixed below the lesser trochanter. The introduction of the subtrochanteric screw in NIS-II may limit the sliding of the fracture site to some extent. The neck screws of PFNA and PFBN are both located at the proximal part of the fracture line of ROTFs. Their neck screws are almost parallel to the main fracture line of ROTFs. This has limited effects on anti-sliding of the proximal fracture fragments for ROTFs.

In this study, we built four fixation models (PFNA, ITN, PFBN, and NIS-II) via finite element method. Finite element analysis (FEA) uses mathematical approximation methods to simulate real physical systems, such as geometric structures, loads, etc. By applying simple and interactive elements, a finite number of unknowns could be used to approximate a real system with infinite unknowns. This method not only has high computational accuracy, but also could adapt to various complex shapes, and has been widely used in the mechanical evaluation of new implants^{17,18}. Three variations of ROTF model (AO/OTA 31-A3) were constructed in this study. Among them, the type of AO/OTA 31-A3.3 represented the most unstable ROTF. The von Mises stress and displacement were tested under axial loads of 2,100 N. Von Mises stress is an equivalent stress used to evaluate the strength of materials under certain load conditions. Our team expected that the NIS-II would provide good biomechanical stability for ROTF patients. Through optimizing stress distribution and reducing displacement of the fracture site, the NIS-II might bring fewer complications and finally improve the prognosis of ROTF patients.

Materials and methods

Three-dimensional (3D) modelling of ROTF

Written informed consents were obtained from the participants, and all methods were performed based on relevant guidelines and regulations. The experimental protocols were approved by the ethics committee of Xi'an Honghui Hospital. For the participants, X-ray images of the intact femur were performed to exclude limb deformities, severe osteoporosis, bone tumors, etc. For further research, 20 participants were involved with a mean weight of about 70 Kg. Their femoral computed tomography (CT) scans (thickness, 0.625 mm; resolution, 512×512 pixels) were achieved and the mean CT values were calculated. In Mimics (Materialize Co., Leuven, Belgium), a 3D femoral model was constructed based on the above CT data. Specifically, cortical and cancellous bones were distinguished according to Hounsfield Unit values and the boundary was set at 700¹⁹. To achieve satisfactory binarization results, the threshold range was fine tuned based on the actual image features. After that, automated segmentation was performed on the basis of the threshold settings and the initial model was generated. The boundary contour of the initial model was optimized by morphological operations. The two dimensional images were inspected one by one. The discovered hollow areas were manually filled. Then, a 3D femoral model was automatically generated based on the previously processed two dimensional images via the Mimics software. The newly created model was converted to STL format and imported into Studio (Geomagic Co., United States) for solidification, including smoothing, denoising, and surface fitting. As shown in Fig. 1E and G, three variations (AO/OTA 31-A3.1, 31-A3.2, and 31-A3.3) of ROTF were established in accordance with previously published fracture map and the 2018 AO/OTA Fracture and Dislocation Classification Guidelines^{2,20}.

Establishing of four implant models

The design of four implants (PFNA, ITN, PFBN, and NIS-II, Fig. 1A and D) was conducted via Computer-Aided Design (CAD) software (Autodesk Co., United States). The formed implant models were subsequently assembled onto the ROTF models, respectively. The four implants possessed the same length (380 mm) and diameter (10 mm). To maintain consistency in neck screw position among these fixation models, the neck screws were inserted in the lower one third of the femoral head for each implant and the tip-apex distance (TAD) value was controlled at approximately 20 mm. For the NIS-II, the diameters of the sleeve, the upper and lower neck screws, and the subtrochanteric screw are defined as 12.0 mm, 6.4 mm, 9.0 mm, and 5.0 mm, respectively. The included angle between the lower neck screw and the main nail is 130 degrees. For the two neck screws, it is set as 7.5 degrees. Besides, the included angle between the subtrochanteric screw and the lower neck screw is defined as 90 degrees.

Mesh convergence and model validation

The mesh type was set as tetrahedral elements in finite element modelling. A mesh convergence test was performed to assess the reliability of finite element models referring to previous research²¹. The maximal von Mises stress on femurs was used for evaluating mesh convergence. The maximal stress on femur models were

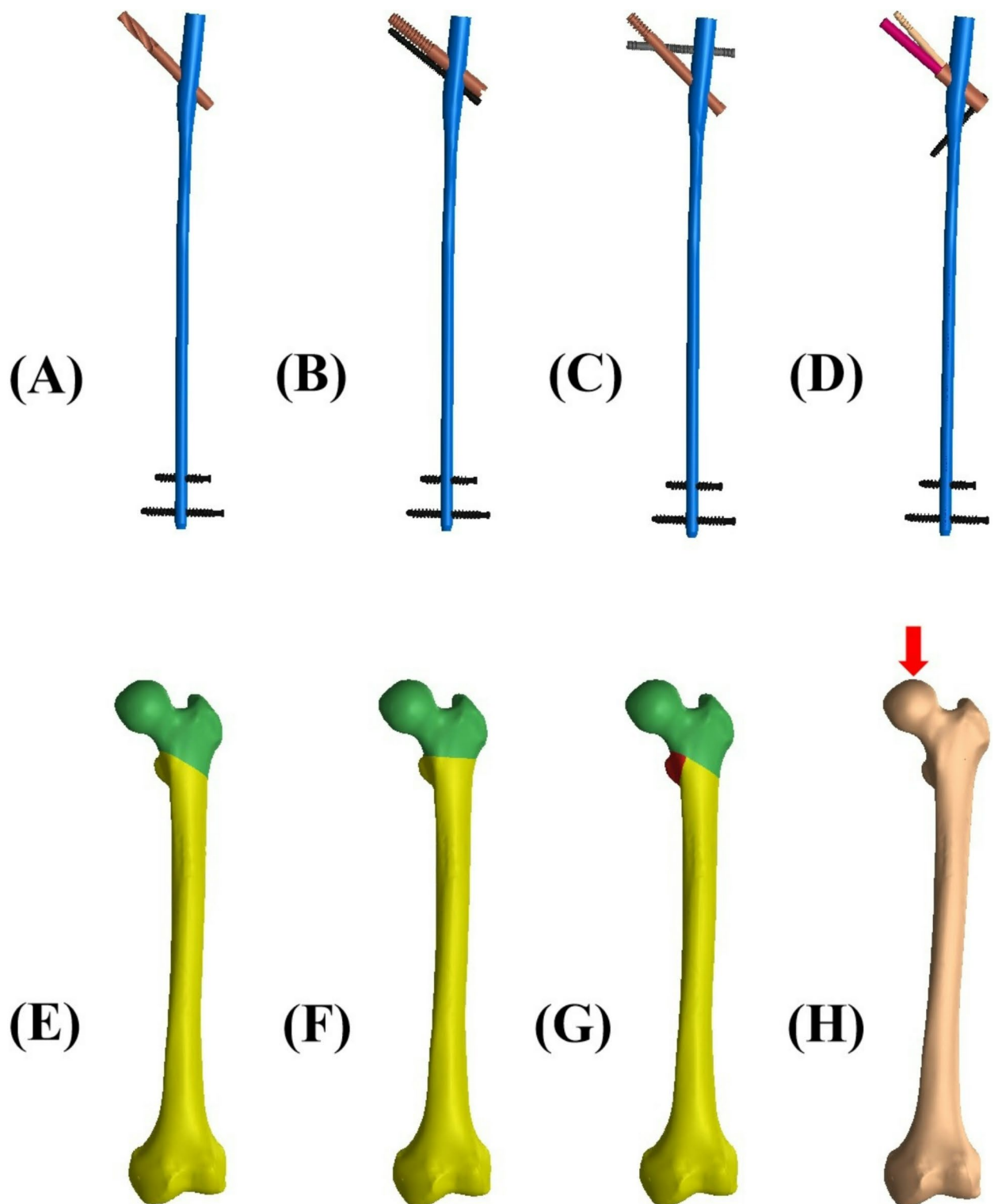


Fig. 1. Intramedullary nail models and the reverse obliquity trochanteric fracture models. (A) PFNA. (B) ITN. (C) PFBN. (D) NIS-II. (E) AO/OTA 31-A3.1 fracture. (F) AO/OTA 31-A3.2 fracture. (G) AO/OTA 31-A3.3 fracture. (H) Schematic diagrams of axial loads. PFNA denotes the Proximal Femoral Nail Antirotation. ITN denotes the InterTAN nail. PFBN denotes the Proximal Femoral Bionic Nail. NIS-II denotes the New Intramedullary System-II.

compared among five mesh sizes. Our data showed that maximal stress on bones at the mesh size of 1.5 mm was close to those of at the 1 mm and 2 mm, and the differences were within 5%. Thus, the mesh size was set as 1.5 mm in this research. With maximal Degree of Freedom, field variables, such as strain energy and displacement, were also within the scope of 5% for both types of elements and there was no maximal stress point. The mesh convergence results proved that the finite element models of this study were reliable.

To conduct model validation, as we have explained earlier, an intact 3D femoral model was constructed through finite element method. The material properties of the femoral model were defined as isotropic, homogeneous, and linear elastic¹⁶. For Young's modulus, it was set as 16,800 MPa for cortex and 840 MPa for cancellous bones¹⁶. In terms of the Poisson's ratio, it was defined as 0.2 for cancellous bones and 0.3 for cortex²². Previous literature have demonstrated that stress applying to the femoral head could be as high as two to three times of one's weight in walking²³. For a patient with a weight of about 70 kg, the peak loads acting on the femoral head are approximately 2,100 N during walking. Therefore, the axial loads of 2,100 N were applied to the femoral head surface to test axial stiffness. Axial stiffness of the intact femur was evaluated by the Ansys19.0 (ANSYS, US) and compared with experimental results published in previous research²⁴. After testing, the axial stiffness of our femur model was 0.63 kN/mm and this value was within the interval (0.76 ± 0.26 kN/mm) of previous cadaveric experiments²⁴. Therefore, the finite element model of our study was validated.

Material properties and boundary settings

As our research focused on the biomechanical stability of implants, soft tissues around the proximal femur were ignored during finite element modelling. To ensure a single variable, material properties were simplified to some extent. Referring to similar studies¹⁶, material properties of the femur and implants were assumed to be isotropic, homogeneous, and linear elastic. The number of elements and nodes for the PFNA, ITN, PFBN, and NIS-II fixation models in three variations of ROTF models was shown in Table 1. The metallic properties of implants were defined as Titanium alloy. In terms of Young's modulus, it was set as 16,800 MPa, 840 MPa, and 110,000 MPa for cortex, cancellous bones and Titanium alloy¹⁶. With regard to the Poisson's ratio, it was 0.2 for cancellous bones while 0.3 for cortex and Titanium alloy referring to previous studies²². All contact types were assumed to be friction contact. The frictional coefficient was set as 0.46 for the bone-bone surface, 0.3 for the bone-implant surface, and 0.2 for implant-implant surface^{25,26}. To simulate vertical compression, the femoral condyle was strictly fixed. Each model was abducted for ten degrees and tilted backward for nine degrees. The single-cycle loads of 2,100 N were loaded on the femoral head of each finite element model vertically (Fig. 1H)²⁵.

Evaluation indicators and statistical analysis

Von Mises stress on implants and bones, maximal displacement of models and fracture surface were calculated to test the stress distribution and mechanical stability of four fixation models. The greater the von Mises stress is, the more concentrated the local stress is, and the easier it is for the implant to rupture at that location. The larger the displacement is, the worse the mechanical stability of the implant is. The PFNA fixation group was set as the control group due to its wide application in fixing femoral trochanteric fractures. The percentage difference (PD) was evaluated according to the following formula: $PD = (P_1 - P_a) / P_1 \times 100\%$. P_a denotes the values of the ITN, PFBN or NIS-II while P_1 denotes the value of PFNA. SPSS 28.0 software (IBM Co., USA) was used to conduct statistical analysis. The displacement and stress values of three ROTF models between the PFNA and NIS-II groups were compared. Student's t-test was used in comparison and $p < 0.05$ was considered as statistically significant.

Results

Maximal displacement for the four fixation models

The cloud images of maximal displacement in axial loads of 2,100 N are displayed in Fig. 2. For the AO/OTA 31-A3.1 (A3.1) fracture, the values of maximal displacement were 17.48 mm, 17.46 mm, 15.45 mm, and 15.91 mm for the PFNA, ITN, PFBN, and NIS-II models, respectively. They were 17.21 mm, 17.45 mm, 15.77 mm, and 15.28 mm for the AO/OTA 31-A3.2 (A3.2) fracture while 17.83 mm, 17.59 mm, 16.99 mm, and 15.96 mm for the AO/OTA 31-A3.3 (A3.3) fracture. The PD reduction of maximal displacement for the NIS-II model relative to the PFNA model was 9.0% in A3.1 fracture, 11.2% in A3.2 fracture, and 10.5% in A3.3 fracture.

Model	A3.1		A3.2		A3.3	
	Nodes	Elements	Nodes	Elements	Nodes	Elements
PFNA	652,619	419,071	652,431	418,851	650,140	417,555
ITN	741,849	471,879	741,418	471,489	740,420	471,104
PFBN	735,859	463,758	736,109	463,921	735,701	463,665
NIS-II	726,505	459,155	725,876	458,727	727,101	459,599

Table 1. Number of nodes and elements for the four fixation models. PFNA denotes the Proximal Femoral Nail Antitotation. ITN denotes the InterTAN nail. PFBN denotes the Proximal Femoral Bionic Nail. NIS-II denotes the New Intramedullary System-II. A3.1 denotes AO/OTA 31-A3.1. A3.2 denotes AO/OTA 31-A3.2. A3.3 denotes AO/OTA 31-A3.3.

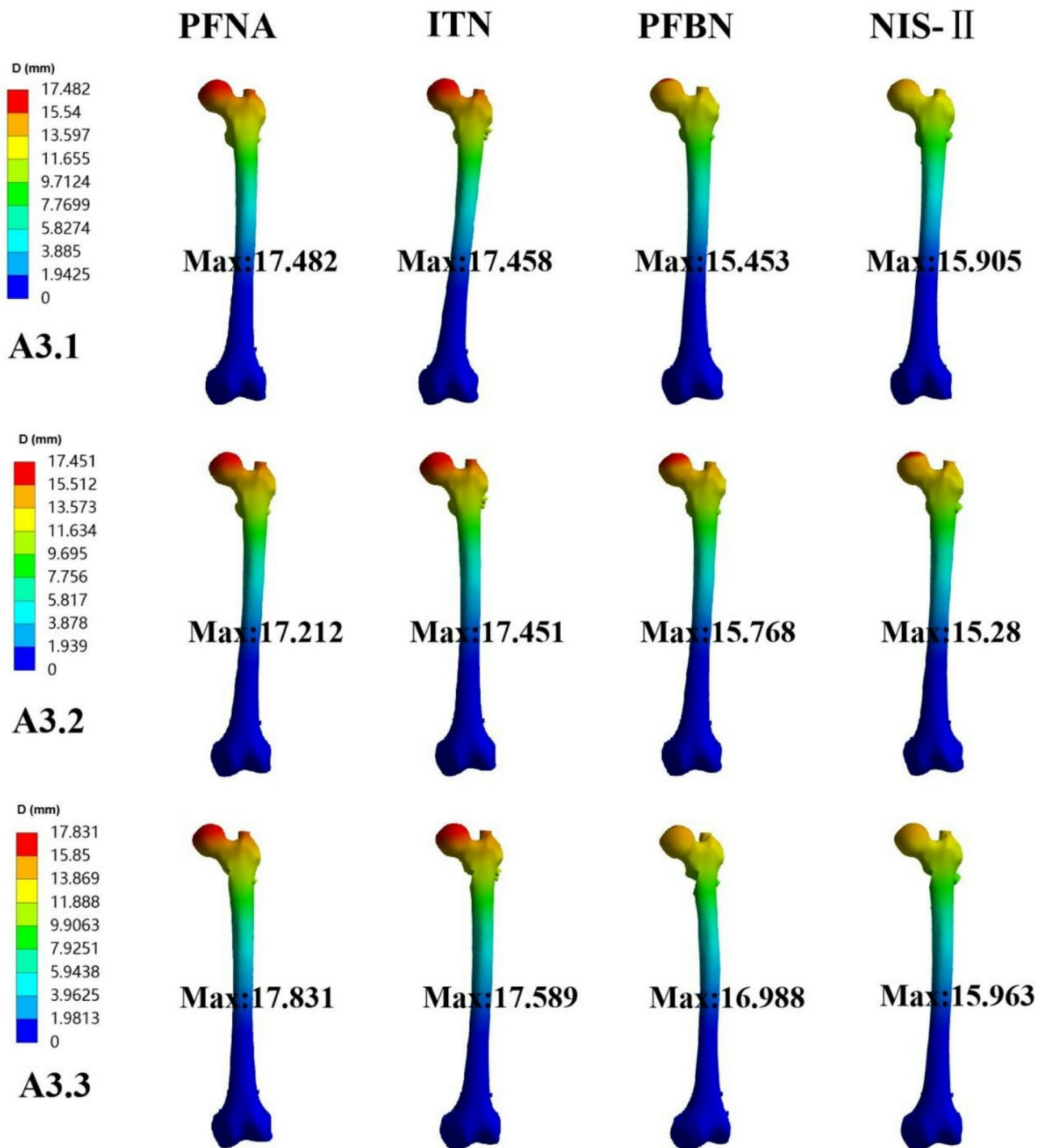


Fig. 2. Maximal displacement for the PFNA, ITN, PFBN, and NIS-II models in A3.1, A3.2, and A3.3 fractures. PFNA denotes the Proximal Femoral Nail Antirotation. ITN denotes the InterTAN nail. PFBN denotes the Proximal Femoral Bionic Nail. NIS-II denotes the New Intramedullary System-II. A3.1 denotes AO/OTA 31-A3.1. A3.2 denotes AO/OTA 31-A3.2. A3.3 denotes AO/OTA 31-A3.3.

Maximal displacement of fracture surface (MDFS) for the four fixation models

The cloud images of MDFS in axial loads of 2,100 N are shown in Fig. 3. The values of MDFS were 12.11 mm, 11.27 mm, 11.83 mm, and 10.91 mm for the PFNA, ITN, PFBN, and NIS-II models in A3.1 fracture, respectively. They were 12.11 mm, 11.93 mm, 11.26 mm and 10.57 mm in A3.2 fracture for the four fixation models. Moreover, the values of this indicator were 12.47 mm, 12.45 mm, 12.02 and 10.93 mm in A3.3 fracture, respectively. The values of MDFS for the NIS-II models were lower than those of the PFNA models in axial load case. Specially,

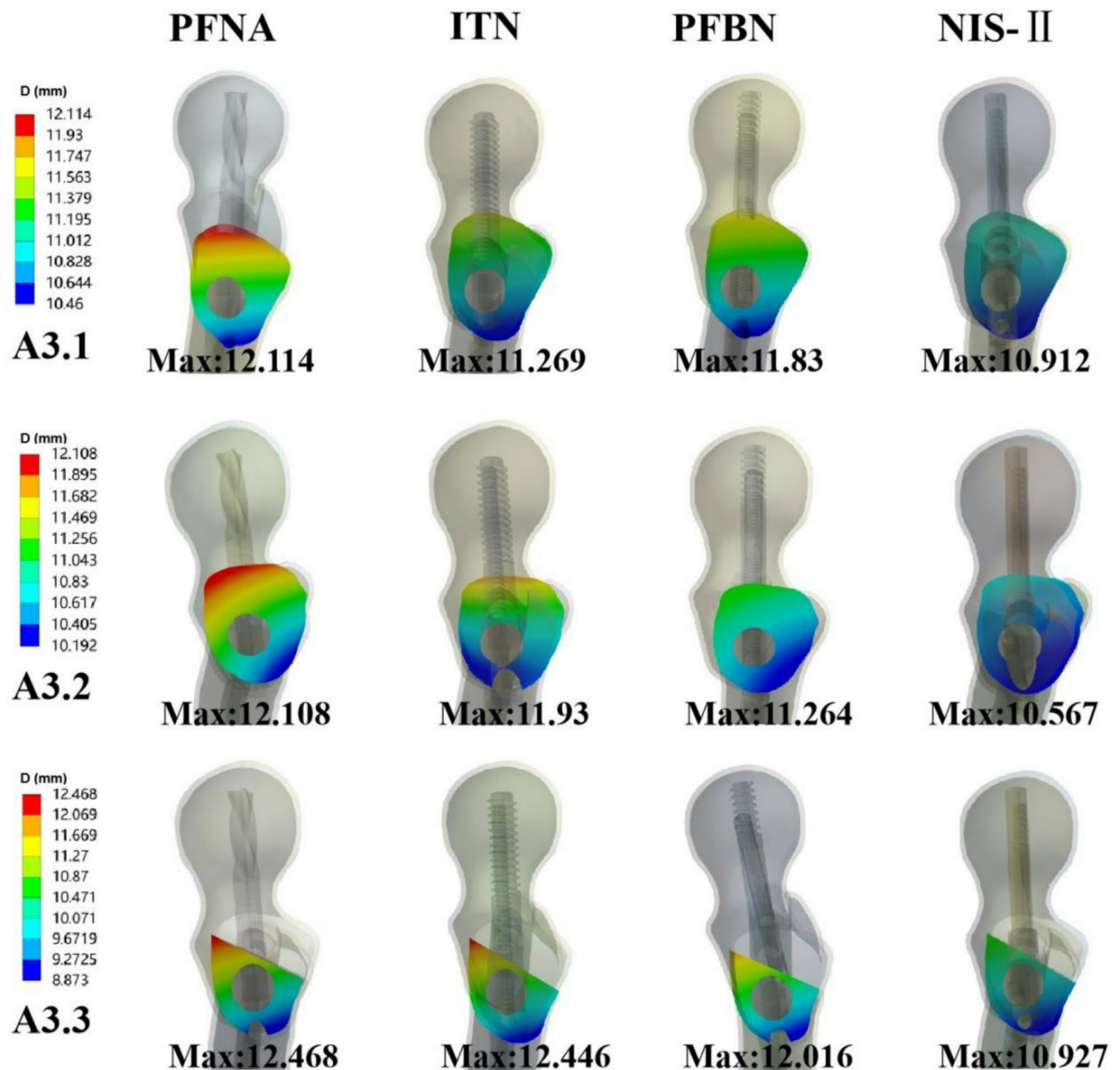


Fig. 3. Maximal displacement of fracture surface for the PFNA, ITN, PFBN, and NIS-II models in A3.1, A3.2, and A3.3 fractures. PFNA denotes the Proximal Femoral Nail Antirotation. ITN denotes the InterTAN nail. PFBN denotes the Proximal Femoral Bionic Nail. NIS-II denotes the New Intramedullary System-II. A3.1 denotes AO/OTA 31-A3.1. A3.2 denotes AO/OTA 31-A3.2. A3.3 denotes AO/OTA 31-A3.3.

compared to the PFNA model, the PD reduction of this indicator for the NIS-II model was 9.9%, 12.7%, and 12.4% in A3.1, A3.2, and A3.3 fractures, respectively.

Maximal stress on implants for the four fixation models

In A3.1 fracture, the maximal stress on implants was 397.01 MPa, 235.69 MPa, 178.38 MPa, and 181.11 MPa for the PFNA, ITN, PFBN, and NIS-II models, respectively. The values were 262.36 MPa, 245.17 MPa, 198.06 MPa, and 131.04 MPa for these models in A3.2 fracture. In addition, they were 496.61 MPa, 158.16 MPa, 270.17 MPa, and 180.32 MPa in A3.3 fracture, respectively. The values of maximal stress on implants for the NIS-II models were lower than those of the PFNA models in three variations of ROTF models. Compared to the PFNA model, the reduction of PD for the NIS-II model was 54.4%, 50.1%, and 63.7% in A3.1, A3.2, and A3.3 fractures, respectively. The cloud images of maximal stress on implants in axial load case are exhibited in Fig. 4.

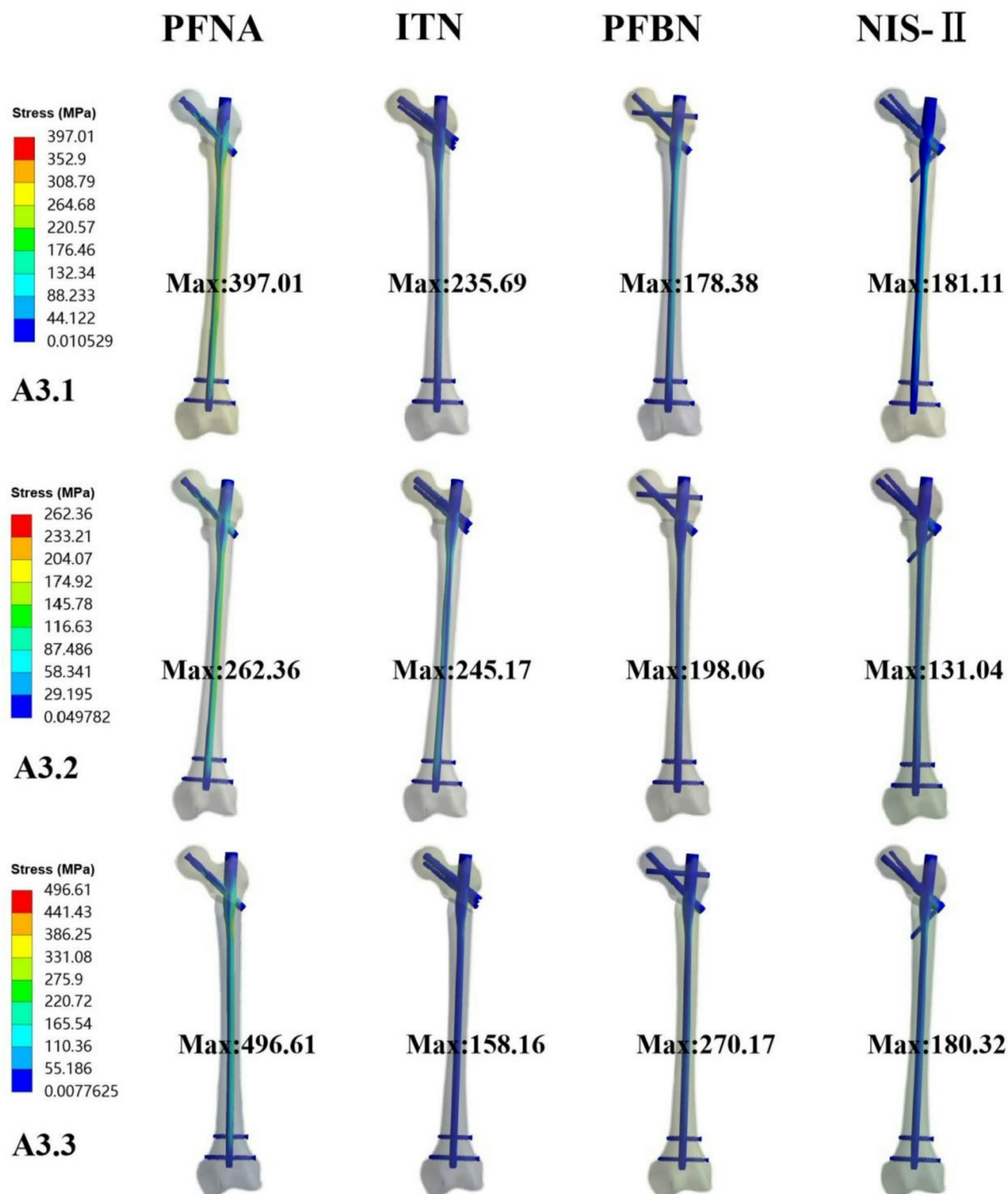


Fig. 4. Maximal stress on implants for the PFNA, ITN, PFBN, and NIS-II models in A3.1, A3.2, and A3.3 fractures. PFNA denotes the Proximal Femoral Nail Antirotation. ITN denotes the InterTAN nail. PFBN denotes the Proximal Femoral Bionic Nail. NIS-II denotes the New Intramedullary System-II. A3.1 denotes AO/OTA 31-A3.1. A3.2 denotes AO/OTA 31-A3.2. A3.3 denotes AO/OTA 31-A3.3.

Maximal stress on bones for the four fixation models

The maximal stress on femurs was 101.24 MPa, 83.12 MPa, 80.13 MPa, and 61.87 MPa for the PFNA, ITN, PFBN, and NIS-II models in A3.1 fracture, respectively. They were 101.38 MPa, 80.03 MPa, 80.42 MPa, and 68.31 MPa for the four fixation models in A3.2 fracture. Besides, the values were 113.80 MPa, 99.04 MPa, 68.44 MPa, and

69.65 MPa in A3.3 fracture, respectively. The values of maximal stress on femurs for the NIS-II models were lower than those of the PFNA models in three variations of ROTF models. Notably, compared to the PFNA model, the PD reduction of this indicator for the NIS-II was 38.9%, 32.6%, and 38.8% in A3.1, A3.2, and A3.3 fractures, respectively. The cloud images of maximal stress on femurs in axial load case are displayed in Fig. 5.

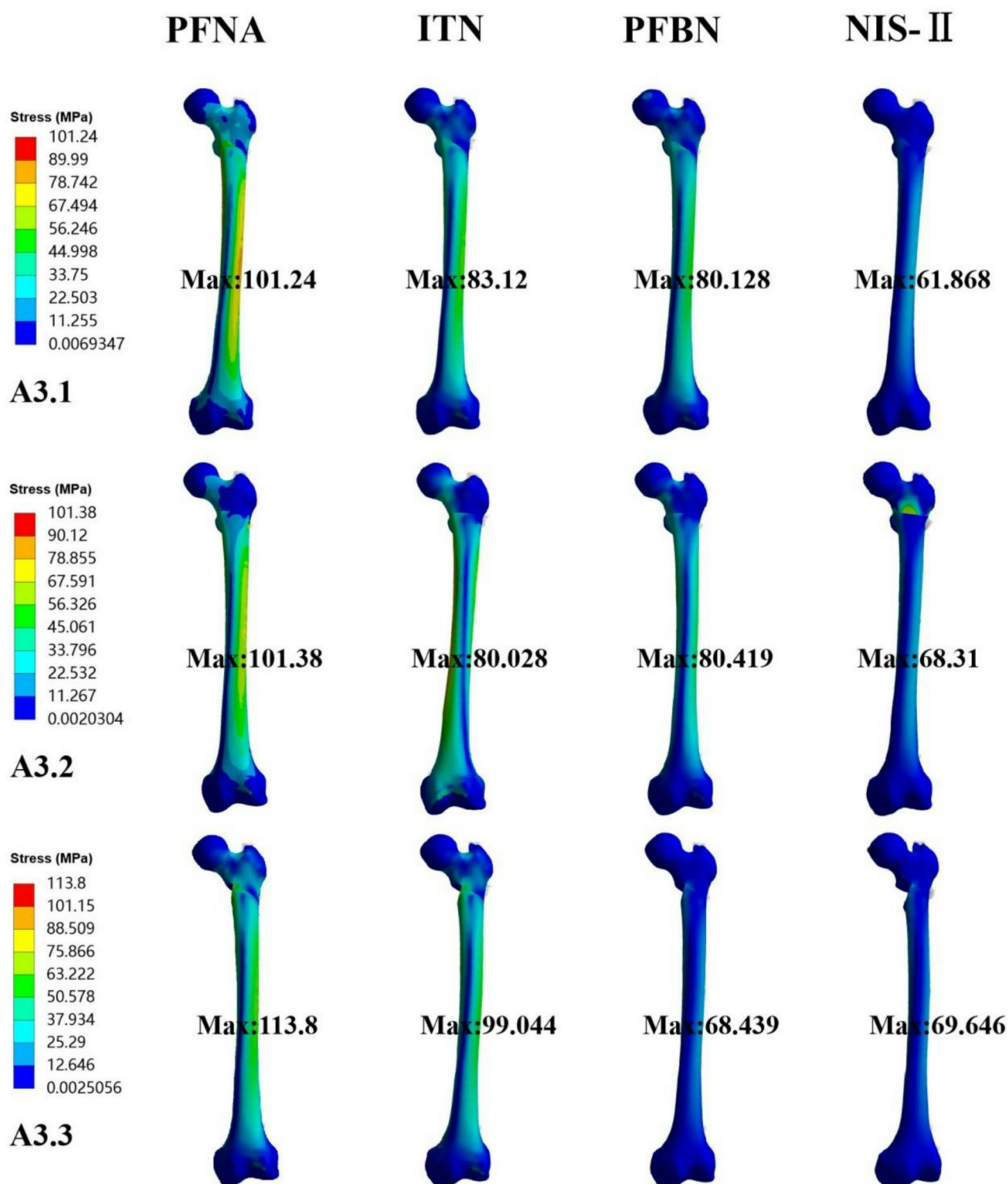


Fig. 5. Maximal stress on bones for the PFNA, ITN, PFBN, and NIS-II models in A3.1, A3.2, and A3.3 fractures. PFNA denotes the Proximal Femoral Nail Antirotation. ITN denotes the InterTAN nail. PFBN denotes the Proximal Femoral Bionic Nail. NIS-II denotes the New Intramedullary System-II. A3.1 denotes AO/OTA 31-A3.1. A3.2 denotes AO/OTA 31-A3.2. A3.3 denotes AO/OTA 31-A3.3.

Evaluation indicators	PFNA	NIS-II	t	p
Maximal displacement (mm)	17.51 ± 0.31	15.72 ± 0.38	6.322	0.008
MDFS (mm)	12.23 ± 0.21	10.80 ± 0.20	8.541	0.003
Maximal stress on implants (MPa)	385.33 ± 117.56	164.16 ± 28.68	3.166	0.087
Maximal stress on bones (MPa)	105.47 ± 7.21	66.61 ± 4.16	8.086	0.004

Table 2. Statistical analysis of evaluation indicators of three ROTFs between PFNA and NIS-II. ROTFs denotes the reverse obliquity trochanteric fractures. PFNA denotes the Proximal Femoral Nail Antirotation. NIS-II denotes the New Intramedullary system-II. MDFS denotes maximal displacement of fracture surface.

Comparison of Biomechanical indicators and statistical analysis

Table 2 showed the statistical results of the PFNA and NIS-II groups in three ROTF models under axial loads of 2,100 N. The mean values of maximal displacement in three ROTF models were 17.51 ± 0.31 mm for the PFNA group and 15.72 ± 0.38 mm for the NIS-II group, and the statistical difference was significant ($p < 0.05$). The mean values of MDFS were 12.23 ± 0.21 mm and 10.80 ± 0.20 mm for the PFNA and NIS-II groups, with significant statistical difference between the two groups ($p < 0.05$). Besides, the mean values of maximal stress on implants were 385.33 ± 117.56 MPa and 164.16 ± 28.68 MPa, and there was no statistical difference ($p > 0.05$). The mean values of maximal stress on bones were 105.47 ± 7.21 MPa and 66.61 ± 4.16 MPa for the PFNA and NIS-II groups, and the statistical difference was significant ($p < 0.05$).

Discussion

In this study, our team compared the mechanical stability of PFNA, ITN, PFBN, and NIS-II for the treatment of reverse obliquity trochanteric fractures via finite element method. Compared to the PFNA model, the NIS-II model proved a 9.0–11.2% reduction in maximal displacement and a 54.4–63.7% reduction in maximal stress on implants. The indicators, including maximal displacement, MDFS, and maximal stress on femurs, showed statistical difference between the PFNA and NIS-II groups ($p < 0.05$). These results indicated that the NIS-II device optimized the stress distribution of the proximal femur of ROTFs. The design of the NIS-II decreased stress concentration of ROTFs and enhanced the overall stability, so as to reduce the risk of fixation failure.

Intramedullary fixation has been the recommended method for managing trochanteric fractures, specially those accompanied by osteoporosis^{6–8,27}. Yet, the effects of traditional intramedullary nails in addressing ROTFs were limited. Irgit et al. included 148 cases with AO/OTA 31-A3 fractures who were treated by intramedullary nails²⁸. Their results showed that 18 patients (12%) suffered postoperative complications and 12 cases (8%) needed re-operations²⁸. For elderly trochanteric fractures, the incidence of these complications might be higher and can cause serious functional impairment. Early surgical intervention of ROTFs is important to decrease long term best-rest complications and reduce the mortality rate²⁹. Traditional intramedullary nails initially experience innovation on the neck screws, such as an increase in number of neck screws or modification of geometric structures to the screw head. These changes provide good mechanical properties to femoral trochanteric fractures, including AO/OTA 31-A1 and 31-A2 types. Yet, when discussing the reverse oblique fractures, known as the AO/OTA 31-A3, the design concept of traditional intramedullary nails may lack the capability to resist the sliding of the proximal fragment to some extent. Hence, the incidence of fixation failure via traditional intramedullary nails remains high²⁸.

The design of NIS-II has been made significant improvements on the basis of traditional intramedullary nails. The unique geometric design of the NIS-II device might be the reasons for its superior mechanical stability compared with PFNA. The corresponding displacement under axial loads reflects the stability of implants. As shown in our research results, the dual-screw design of ITN, PFBN, and NIS-II showed lower maximal displacement and MDFS values than that of the single-screw of PFNA. This meant that the ITN, PFBN, and NIS-II provided better mechanical stability under vertical loads than that of the PFNA. In NIS-II, one significant difference from the ITN and PFBN is the introduction of the subtrochanteric screw. From the perspective of subtle structure, a triangular stable structure is formed by the subtrochanteric screw, the sleeve, and the main nail in NIS-II. This design might provide good stability for the fracture site, thereby reducing displacement of the fracture site. When using traditional intramedullary nails, such as PFNA, to fix ROTFs, the neck screw is almost parallel to the main fracture line, which could easily lead to complications such as screw cutout, femoral displacement, and implant break. The interlocking of the subtrochanteric screw and the sleeve limits the sliding of the proximal fragment in ROTFs to the most extent. Besides, in traditional intramedullary nails, the junction between the neck screw and the main nail is a stress concentration area. Compared with PFNA, ITN, and PFBN, the NIS-II fixation model displayed lower maximal stress values on implants under axial loads of 2,100 N. The subtrochanteric screw of NIS-II dispersed the stress at the junction between the sleeve and the main nail. These characteristics might result in fewer fixation failures for the NIS-II than that of PFNA. As known to all, the PFBN is a relatively new internal implant for the treatment of trochanteric fractures whose design concept was also on the basis of triangular stability theory¹⁰. Previous researches indicated that compared to the PFNA and ITN, the PFBN device possessed better biomechanical stability in addressing AO/OTA 31-A1.3 and 31-A3 fractures^{10,11}. However, the triangular structure of PFBN is distributed above the main fracture line of ROTFs, so it might not bring superior anti-sliding features for ROTFs. Unlike this, the neck screws and the subtrochanteric screw of the NIS-II are distributed at both sides of the main fracture line of ROTFs, and they are interlocked via a right angle. The main fracture line of ROTFs seems to be “locked” in this triangular structure. Compared to other intramedullary nails (PFNA, ITN, and PFBN), the NIS-II exhibited lower maximal displacement values under

axial loads. This fully demonstrated that the NIS-II device did provide good anti-sliding effects and its design was reasonable. Through the unique design, NIS-II might ultimately reduce the fixation failure rate of ROTFs.

The medial support of proximal femur is a vital factor for the management of trochanteric fractures^{30–32}. In a study by Chen et al., the reduction loss rate postoperatively resulting from comminuted medial wall was as high as 20% in femoral trochanteric fractures³⁰. Song et al. reported that the comminuted medial wall of proximal femur was a reliable index to predict fixation failure after using intramedullary nails for patients with trochanteric fractures³¹. Other scholars proved that the medial wall was more important than the lateral wall for the fixation of femoral trochanteric fractures³². The medial support nail-II (MSN-II) was specially designed for fixing ROTFs based on medial support theory³³. In the finite element study by Nie et al., the MSN-II showed better biomechanical properties in addressing ROTFs under increasing axial loads, compared to the PFNA-II¹⁶. Even though the MSN-II contains two neck screws (an axial neck screw and a short medial support screw), they are nearly parallel to the main fracture line of ROTFs. Therefore, the design of MSN-II might limit its anti-sliding function. Notably, the introduction of the subtrochanteric screw in NIS-II brings an effective solution for providing medial support. The subtrochanteric screw could be fixed from the lateral to the medial region of the proximal femur in a direction almost perpendicular to the main fracture line of ROTFs. The cloud images and comparison of displacement data for four fixation models in our study confirmed this point.

There are still several limitations about this study. Firstly, the bone and implant materials were assumed to be homogeneous, isotropic, and linear elastic. In reality, bone demonstrates anisotropic and viscoelastic properties. This may potentially affect our finite element outcomes. Yet, to ensure a single variable, this simplification was reasonable to some extent. Secondly, the loads acting on the femoral head are usually complex in real-world, and vertical compression is just one of the common types. Further research is needed on more complex or dynamic load models. Thirdly, in this study, the soft tissue situations were not simulated. As our research focused on the mechanical properties of metal implants, their interaction with bone tissues was the most important factor. Therefore, it was necessary to ignore the influence of soft tissues. Fourthly, due to resolution limitations, there may be some deviation in the results displayed by the cloud images, which might affect our interpretation of the results to some extent. Fifthly, although our team has confirmed the good mechanical properties of NIS-II through finite element modelling, further cadaver experiments and clinical studies are still necessary.

Conclusion

The New Intramedullary System-II showed the most superior stress distribution and the overall mechanical stability, followed by PFBN, ITN, and PFNA in fixing reverse obliquity trochanteric fractures under axial loads. Accordingly, the design of NIS-II is feasible and this implant could be a new choice for the treatment of ROTFs. It might decrease the fixation failure rate of ROTFs in clinical application.

Data availability

The datasets analyzed during the current study are available from the corresponding author upon reasonable request.

Received: 10 December 2024; Accepted: 5 May 2025

Published online: 14 May 2025

References

- Haidukewych, G. J., Israel, T. A. & Berry, D. J. Reverse obliquity fractures of the intertrochanteric region of the femur. *J. Bone Joint Surg. Am.* **83**, 643–650 (2001).
- Meinberg, E. G., Agel, J., Roberts, C. S., Karam, M. D. & Kellam, J. F. Fracture and dislocation classification compendium-2018. *J. Orthop. Trauma*. **32**, S1–S10 (2018).
- Park, S. Y., Yang, K. H., Yoo, J. H., Yoon, H. K. & Park, H. W. The treatment of reverse obliquity intertrochanteric fractures with the intramedullary hip nail. *J. Trauma*. **65**, 852–857 (2008).
- Honkonen, S. E., Vihtonen, K. & Jarvinen, M. J. Second-generation cephalomedullary nails in the treatment of reverse obliquity intertrochanteric fractures of the proximal femur. *Injury* **35**, 179–183 (2004).
- Makki, D., Matar, H. E., Jacob, N., Lipscombe, S. & Gudena, R. Comparison of the reconstruction trochanteric antigrade nail (TAN) with the proximal femoral nail antirotation (PFNA) in the management of reverse oblique intertrochanteric hip fractures. *Injury* **46**, 2389–2393 (2015).
- Tai, D., Chou, S., Taylor, A. M. & Moran, C. G. Reverse oblique intertrochanteric femoral fractures treated with the intramedullary hip screw (IMHS). *Injury* **43**, 817–821 (2012).
- Ozkan, K., Eceviz, E. & Unay, K. Treatment of reverse oblique trochanteric femoral fractures with proximal femoral nail. *Int. Orthop.* **35**, 595–598 (2011).
- Matre, K. et al. Sliding hip screw versus IM nail in reverse oblique trochanteric and subtrochanteric fractures. A study of 2716 patients in the Norwegian hip fracture register. *Injury* **44**, 735–742 (2013).
- Hao, Y. et al. Risk factors for implant failure in reverse oblique and transverse intertrochanteric fractures treated with proximal femoral nail antirotation (PFNA). *J. Orthop. Surg. Res.* **14**, 350 (2019).
- Wang, Y. et al. Finite element analysis of proximal femur bionic nail (PFBN) compared with proximal femoral nail antirotation and intertan in treatment of intertrochanteric fractures. *Orthop. Surg.* **14**(9), (2022).
- Yang, Y. J. et al. Comparative study of a novel proximal femoral bionic nail and three conventional cephalomedullary nails for reverse obliquity intertrochanteric fractures: A finite element analysis. *Front. Bioeng. Biotechnol.* **12** (0), 1393154 (2024).
- Kennedy, M. T. et al. Subtrochanteric hip fractures treated with cerclage cables and long cephalomedullary nails: A review of 17 consecutive cases over 2 years. *Int. J. Care Inj.* **42** (11), 1317–1321 (2011).
- Kilinc, B. E., Oc, Y., Kara, A. & Ertur, R. E. The effect of the cerclage wire in the treatment of subtrochanteric femur fracture with the long proximal femoral nail: A review of 52 cases. *Int. J. Surg.* **56**, 250–255 (2018).
- Karayannis, P. & James, A. The impact of cerclage cabling on unstable intertrochanteric and subtrochanteric femoral fractures: A retrospective review of 465 patients. *Eur. J. Trauma. Emerg. Surg.* **46** (5), 969–975 (2020).
- Hantouly, A. T. et al. The role of cerclage wiring in the management of subtrochanteric and reverse oblique intertrochanteric fractures: A meta-analysis of comparative studies. *Eur. J. Orthop. Surg. Traumatol.* **33** (4), 739–749 (2023).

16. Bai, H. A. et al. Biomechanical evaluation of three implants for treating unstable femoral intertrochanteric fractures: Finite element analysis in axial, bending and torsion loads. *Front. Bioeng. Biotechnol.* **11**, 1279067 (2023).
17. Liu, J., Zhang, Z., Li, P. & Piao, C. Enhancing fixation stability in proximal humerus fractures: screw orientation optimization in PHILOS plates through finite element analysis and Biomechanical testing. *Sci. Rep.* **14**, 27064 (2024).
18. Cui, Y. et al. Biomechanical optimization of the magnesium alloy bionic cannulated screw for stabilizing femoral neck fractures: A finite element analysis. *Front. Bioeng. Biotechnol.* **12**, 1448527 (2024).
19. Abdul Wahab, A. H., Wui, N. B., Kadir, A., Ramlee, M. H. & M. R., & Biomechanical evaluation of three different configurations of external fixators for treating distal third tibia fracture: Finite element analysis in axial, bending and torsion load. *Comput. Biol. Med.* **127**, 104062 (2020).
20. Li, M. et al. Threedimensional mapping of intertrochanteric fracture lines. *Chin. Med. J. Engl.* **132** (21), 2524–2533 (2019).
21. Ding, K. et al. Proximal femoral bionic nail—a novel internal fixation system for the treatment of femoral neck fractures: A finite element analysis. *Front. Bioeng. Biotechnol.* **11**, (2023).
22. Li, J., Zhao, X., Hu, X., Tao, C. & Ji, R. A theoretical analysis and finite element simulation of fixator-bone system stiffness on healing progression. *J. Appl. Biomater. Funct. Mater.* **16**, 115–125 (2018).
23. Bergmann, G. et al. Hip contact forces and gait patterns from routine activities. *J. Biomech.* **34**, 859–871 (2001).
24. Papini, M., Zdero, R., Schemitsch, E. H. & Zalzal, P. The biomechanics of human femurs in axial and torsional loading: Comparison of finite element analysis, human cadaveric femurs, and synthetic femurs. *J. Biomech. Eng.* **129** (1), 12–19 (2007).
25. Xia, Y. et al. Biomechanical study of two alternative methods for the treatment of vertical femoral neck fractures—a finite element analysis. *Comput. Methods Progr. Biomed.* **211**, 106409 (2021).
26. Yang, A. L. et al. Computational evaluation of the axis-blade angle for measurements of implant positions in trochanteric hip fractures: A finite element analysis. *Comput. Biol. Med.* **158**, 106830 (2023).
27. D'Arrigo, C. et al. Intertrochanteric fractures: Comparison between two different locking nails. *Int. Orthop.* **36**, 2545–2551 (2012).
28. Irgit, K. et al. Reverse oblique and transverse intertrochanteric femoral fractures treated with the long cephalomedullary nail. *J. Orthop. Trauma.* **29** (9), e299–304 (2015).
29. Zehir, S., Zehir, R., Zehir, S., Azboy, I. & Haykir, N. Proximal femoral nail antirotation against dynamic hip screw for unstable trochanteric fractures; A prospective randomized comparison. *Eur. J. Trauma. Emerg. Surg.* **41**, 393–400 (2015).
30. Chen, S. Y. et al. A new fluoroscopic view for evaluation of anteromedial cortex reduction quality during cephalomedullary nailing for intertrochanteric femur fractures: The 30 oblique tangential projection. *BMC Musculoskelet. Disord.* **21** (1), 719 (2020).
31. Song, H., Chang, S. M., Hu, S. J., Du, S. C. & Xiong, W. F. Calcar fracture gaping: A reliable predictor of anteromedial cortical support failure after cephalomedullary nailing for Pertrochanteric femur fractures. *BMC Musculoskelet. Disord.* **23** (1), 175 (2022).
32. Nie, B., Chen, X., Li, J., Wu, D. & Liu, Q. The medial femoral wall can play a more important role in unstable intertrochanteric fractures compared with lateral femoral wall: A Biomechanical study. *J. Orthop. Surg. Res.* **12**, 197 (2017).
33. Nie, S. B. et al. Medial support nail and proximal femoral nail antirotation in the treatment of reverse obliquity inter-trochanteric fractures (Arbeitsgemeinschaft für osteosynthesfragen/orthopedic trauma association 31-A3.1): A finite-element analysis. *Chin. Med. J. (Engl)* **133**(22), (2020).

Acknowledgements

None.

Author contributions

Q.H. designed the study. Q. H., Q. W, L. L., K. Z. and Z. L. searched relevant clinical data, analyzed and interpreted the data. Q. W. wrote the manuscript. H. Q. and K. Z. contributed most in the revision of this manuscript. All authors approved the final version of the manuscript.

Funding

This study was supported by the Bureau project of Xi'an Health Commission (2024ms08). The funding source has no role in study design, conduction, data collection or statistical analysis.

Declarations

Competing interests

The authors declare no competing interests.

Consent to participate/Consent to publish

All patients or their family members have signed the informed consent before surgery and provided the consent to publish and report individual clinical data.

Additional information

Correspondence and requests for materials should be addressed to Q.H.

Reprints and permissions information is available at www.nature.com/reprints.

Publisher's note Springer Nature remains neutral with regard to jurisdictional claims in published maps and institutional affiliations.

Open Access This article is licensed under a Creative Commons Attribution-NonCommercial-NoDerivatives 4.0 International License, which permits any non-commercial use, sharing, distribution and reproduction in any medium or format, as long as you give appropriate credit to the original author(s) and the source, provide a link to the Creative Commons licence, and indicate if you modified the licensed material. You do not have permission under this licence to share adapted material derived from this article or parts of it. The images or other third party material in this article are included in the article's Creative Commons licence, unless indicated otherwise in a credit line to the material. If material is not included in the article's Creative Commons licence and your intended use is not permitted by statutory regulation or exceeds the permitted use, you will need to obtain permission directly from the copyright holder. To view a copy of this licence, visit <http://creativecommons.org/licenses/by-nc-nd/4.0/>.

© The Author(s) 2025